On the Most Informative Slice of Bicoherence That Characterizes Resting State Brain Connectivity

Ahmet Levent Kandemir
Graduate School of Informatics
Middle East Technical University
Ankara, Turkey
levent.kandemir@metu.edu.tr

Tolga Esat Özkurt
Graduate School of Informatics
Middle East Technical University
Ankara, Turkey
ozkurt@metu.edu.tr

***Abstract*—Bicoherence is a useful tool to detect nonlinear interactions within the brain with high computational cost. Latest attempts to reduce this computational cost suggest calculating a particular 'slice' of the bicoherence matrix. In this study, we investigate the information content of the bicoherence matrix in resting state. We use publicly available Human Connectome Project data in our calculations. We show that the most prominent information of the bicoherence matrix is concentrated on the main diagonal, i.e., f_1=f_2.**

Keywords—bicoherence, connectivity, quadratic phase coupling, cross-frequency coupling, neural oscillations

I. Introduction

Functional connectivity is described as the integration of segregated brain areas to operate as a network in several task-related and resting state activations [1]. Over the last decades, several empirical studies have shown that the oscillatory synchronization is the key mechanism to functional connectivity between spatially distant areas and quantificiation of oscillatory synchronization is a useful tool to evaluate functioning of pathological and normal brain [2 - 4].

Functional connectivity may be investigated in means of both linear and nonlinear interactions. Linear interactions within the brain have well been studied using the metric of coherence [5, 6]. But linear approaches have limitations since brain is evaluated as a nonlinear and dynamical system [7]. Consequently, various phase estimation and cross-frequency measures are used frequently to investigate functional connectivity caused by nonlinear systems [8 - 11].

A subtype of nonlinear interactions, named quadratic phase coupling (QPC) is an interaction of three frequencies; f_1, f_2 and $f_1 + f_2$. In order to suggest a QPC interaction, sum of the phases at $f_1(\phi_1)$ and $f_2(\phi_2)$ should be the phase at frequency $f_1 + f_2$ $(\phi_1 + \phi_2)$ [12]. Bicoherence is a powerful tool to detect QPC and has been applied successfully to evaluate QPC types of nonlinear interactions in many signal processing fields as well as in human EEG and MEG [13 - 15].

Although proven useful in many signal processing fields, bicoherence has not been used widely in neuroscience due to computational costs [16, 17]. A pairwise bicoherence analysis of multivariate source data requires estimates in the order of $\sim N^2 \times M^2$, where N and M denote the number of channels and the number of sampled frequencies, respectively. In order to reduce computational costs, new methods were suggested. Sensor level PCA was applied by [17] to reduce the data. This approach actually only reduces the computational cost if only the sensor level bicoherence is being calculated. It is not applicable to source level bicoherence calculation. On the other hand, 'sliced bicoherence' was proposed by Özkurt [16] in order to reduce the computational costs with the idea that the most prominent interactions may be located on the main diagonal of bicoherence matrix.

Considering earlier studies on bicoherence, information content of the main diagonal gains importance [16]. For example, a study on monkeys performing visuomotor tasks showed peaks at beta band on main diagonal [18]. A resting state analysis study by Chella et al. [17] identified significant peaks at alpha band particularly on the main diagonal. Similarly, (10-10 Hz) coupling at resting state was highlighted by another study [19]. Diagonal slice may also play a prominent role in the characterization of anesthesia [20]. Nevertheless, the information content of the bicoherence has not been thoroughly demonstrated, yet.

This study examines the bicoherence matrix on resting state data, implements a statistical analysis method to compare diagonal and non-diagonal components and evaluates the efficiency of 'sliced bicoherence' metric. Throughout this paper, the term 'slice' will be used to describe diagonals with the 1st slice being the main diagonal. The indices of the slices increase towards lower left of the matrix. Fig. 1 shows the order of slices.

$$\begin{bmatrix} 1 & . & . & . & . \\ 2 & 1 & . & . & . \\ 3 & 2 & 1 & . & . \\ 4 & 3 & 2 & 1 & . \\ 5 & 4 & 3 & 2 & 1 \end{bmatrix}$$

Fig. 1. 'Slice' Sequence of Bicoherence Matrix.

II. Methods

A. MEG Data

We used resting-state MEG recordings collected in the scope of HCP [21]. They are part of publicly available S1200 release. Details of the scanning procedures and data preprocessing are

ISBN 978-90-827970-1-5

provided by the S1200 Release Reference Manual [22]. Data consist of 89 MEG subjects which are young adults (ages 22-25) with a subset of ~50 same-sex twin pairs.

All subjects were scanned with a whole head Magnes 3600 Scanner (4D Neuroimaging, San Diego, CA, USA) in a magnetically shielded room. Subjects were also scanned with 3T MRI (Siemens 3T "Connectome Skyra", St. Louis, MO, USA) scanner in order to acquire anatomical information. Magnes 3600 system includes 248 MEG channels together with 23 reference channels. In order to co-register MEG data to the MRI scans, a 3-point reference system (nasion and two peri-auricular points) and locator coils were used.

Resting state MEG data were recorded in 3 consecutive sessions for each subject for approximately 6 min. We selected one of three sessions randomly for this study. The data provided with HCP is preprocessed, resampled at 508.625 Hz. and saved in Fieldtrip file format. Bad channels, bad segments and remaining artifacts were removed using ICA. Cardiac components and eye-blinks were also suppressed in this manner.

B. Software and Auxiliary Toolboxes

All of the calculations in this study were implemented in MATLAB® (R2017a, The Mathworks Inc., Natick, MA). Publicly available Fieldtrip Toolbox [23], Higher Order Spectral Analysis (HOSA) Toolbox [24] and MEG Connectome Pipelines [22] were also utilized.

C. Parcellation Atlas

In order to reduce the data, identify Anatomical Volumes of Interest (AVOI) and create group level results, Automated Anatomical Labelling (AAL) Atlas was used [25]. Original AAL Atlas includes 45 AVOIs in each hemisphere reaching a total of 90 AVOIs. AAL Atlas used in this study is based on the original atlas with addition of cerebellum and vermis (Neurofunctional Imaging Group-GIN, UMR6232, CYCERON, Caen, France). Table 1 and Fig. 3 provide detailed information about the atlas used in this study.

D. Data Processing

The workflow of data processing in the scope of this study is given at Fig. 2.

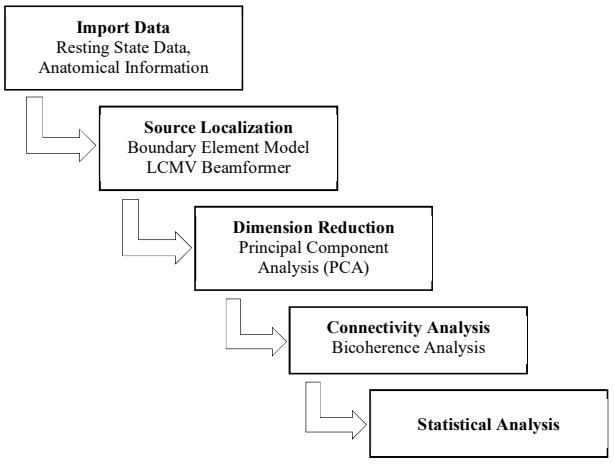

Fig. 2. Workflow of the study given in detail.

(i) Source Localization: For source localization, leadfield matrix was calculated using subject specific headmodel provided by HCP and a 10 mm grid neural source model. Neural source model of ~1500 voxels was created for each subject with subject specific MRI data. Leadfield matrix was reduced to 1 dipole orientation with most variance for each voxel using Single Value Decomposition. Source construction was realized using Linearly Constrained Minimum Variance Beamformer (LCMV) [26].

TABLE I

ANATOMICAL VOLUMES OF INTEREST. GIVEN VOLUME OF EACH AVOI IN THE TABLE IS THE RATIO OF THE TOTAL VOLUME OF THE AVOI IN BOTH HEMISPHERES TO TOTAL VOLUME OF THE BRAIN. GIVEN DISTANCE IS THE DISTANCE OF THE CENTER OF GRAVITY OF EACH AVOI TO THE CLOSEST MEG CHANNEL.

AVOI	AVOI Name	Vol. (%)	Dist. (mm)
1	Precentral	2,68	42,04
2	Frontal_Sup	2,47	55,82
3	Frontal_Sup_Orb	0,34	68,37
4	Frontal_Mid	4,32	51,46
5	Frontal_Mid_Orb	0,96	56,46
6	Frontal_Inf_Oper	1,37	48,21
7	Frontal_Inf_Tri	2,33	49,36
8	Frontal_Inf_Orb	1,92	56,31
9	Rolandic_Oper	1,10	53,01
10	Supp_Motor_Area	1,65	48,84
11	Olfactory	0,27	87,89
12	Frontal_Sup_Medial	3,23	54,19
13	Frontal_Med_Orb	1,17	69,69
14	Rectus	0,69	85,30
15	Insula	1,51	61,22
16	Cingulum_Ant	1,37	70,46
17	Cingulum_Mid	2,68	63,78
18	Cingulum_Post	0,41	83,16
19	Hippocampus	0,89	78,33
20	ParaHippocampal	0,89	83,03
21	Amygdala	0,21	82,63
22	Calcarine	2,40	68,94
23	Cuneus	1,65	58,86
24	Lingual	2,06	75,87
25	Occipital_Sup	1,44	55,47
26	Occipital_Mid	2,81	53,52
27	Occipital_Inf	1,10	53,72
28	Fusiform	2,40	75,03
29	Postcentral	3,16	43,99
30	Parietal_Sup	0,96	42,77
31	Parietal_Inf	1,78	44,19
32	SupraMarginal	1,78	44,81
33	Angular	1,65	48,21
34	Precuneus	3,09	60,04
35	Paracentral_Lobule	0,55	39,30
36	Caudate	0,62	83,09
37	Putamen	0,96	72,20
38	Pallidum	0,21	85,70
39	Thalamus	1,10	86,07
40	Heschl	0,27	72,59
41	Temporal_Sup	2,81	51,12
42	Temporal_Pole_Sup	1,37	54,92
43	Temporal_Mid	4,80	53,82
44	Temporal_Pole_Mid	1,24	57,28
45	Temporal_Inf	2,61	58,14
46	Cerebellum	7,69	58,66
47	Vermis	1,03	62,03

ISBN 978-90-827970-1-5 © EURASIP 2018

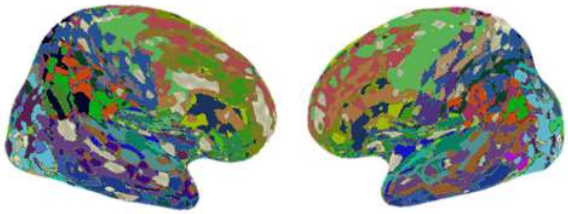

Fig. 3. Representation of AAL Atlas. Different colors are used for separate AVOIs.

(ii) Dimension Reduction: Source level data dimension was reduced using PCA. AAL Atlas was used to separate the data into 116 anatomical volumes of interest. PCA reduction was carried out in a way that each region preserved 90% of its information. Depending on the information content of the region, some regions preserved more than one time-series. The number of virtual time-series is subject specific, ranging from 210 to 280 with the average of ~250. Fig. 4. shows an exemplary PCA Dimension Reduction.

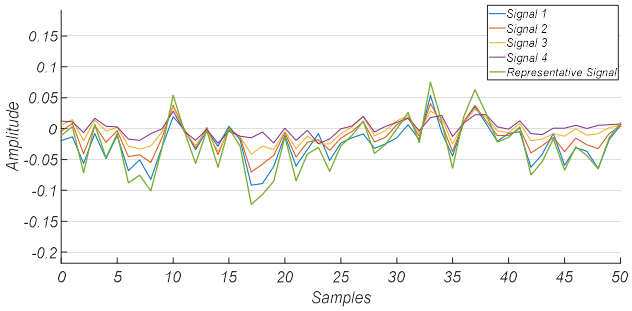

Fig. 4. Dimension Reduction Using PCA. An exemplary AVOI is shown for visualization. PCA was used to reduce four source-space signals in an AVOI to a single representative signal.

(iii) Bicoherence Estimation: HOSA Toolbox [24] was used for bicoherence estimation in this study. Data were segmented into non-overlapping 256 sample Hanning windows. The mean was removed from each record and the Fast Fourier Transform was computed. Both window type and window length reduce the frequency resolution of Discrete Fourier Transform, leading to a 4 Hz of spectral resolution limit. However, for the sake of brevity and proper display, during calculations, number of FFT points was set to sampling frequency, leading to 1 Hz of visible frequency resolution in figures. This is achieved by interpolation method applied by Matlab's 'fft' implementation. For each subject, bicoherence matrix was calculated $N \times N$ times where N is the number of virtual time series. Calculation of cross bicoherence between time-series $x(t)$ and $y(t)$ is given as below;

$$b_{ij} = \frac{|E\{X(f_1)X(f_2)Y^*(f_1+f_2)\}|^2}{S_X(f_1)S_X(f_2)S_Y(f_1+f_2)} \qquad (1)$$

where superscript $*$ denotes complex conjugate and $E\{\}$ is the statistical expectation operator [27]. Here, X and S denote Fourier coefficients and spectra respectively.

(iv) Confidence Level Calculation and Acquisition of Bicoherence Matrices: An empirical confidence level for each subject was calculated using Bootsrapping Resampling Method [28]. Randomly chosen 5 virtual time-series pair was used for calculation. For each pair, one of the signals was divided into 256 sample pieces and shuffled 100 times to calculate bicoherence repeatedly. As a result, 500 different bicoherence matrices were produced for each subject. For each frequency pair, the 95% limit of the distribution of 500 values was assigned as the confidence level for that particular frequency pair of the processed subject. Acquired confidence level matrix was used for each subject to threshold the calculated bicoherence matrices. Values of frequency pairs above confidence level were accepted significant and represented with '1'. The remaining values were assigned '0', making a binary matrix. Entire sets of bicoherence matrices calculated for each subject were used to calculate the percentage of significant bicoherence of each frequency pair. Calculated Bicoherence results and confidence level matrices are averaged across subjects for evaluations.

(v) Statistical Analysis: We averaged the values of diagonal (128 elements) and non-diagonal (8128 elements) components separately. One-tailed t-test was used with the hypothesis that there is more nonlinear interaction at the main diagonal slice than there is at the non-diagonal slices.

III. Results

Averaged bicoherence matrix across subjects is given at Fig. 5. Results show that there are several important interactions within and cross frequency bands. Each pixel in the matrix represents information content of each frequency bin (128×128) in terms of percentage of significant bicoherence. Frequency bins greater than (35-35 Hz.) are disregarded due to low or no information. As expected at resting state data, the most prominent interaction is visual at the alpha band (8-12 Hz.).

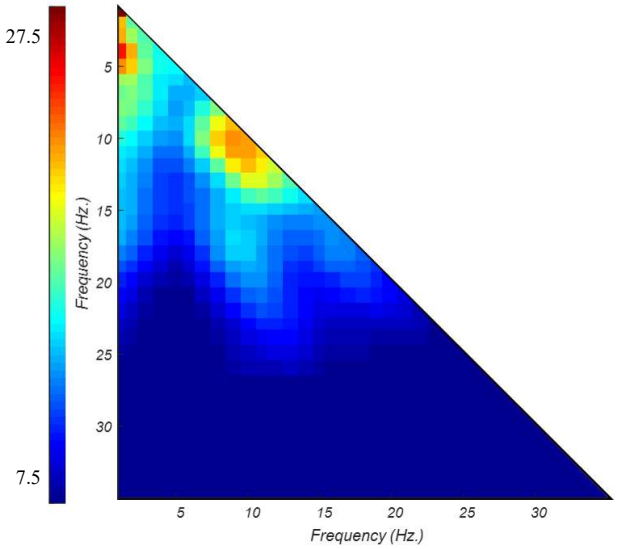

Fig. 5. Total Bicoherence Results. Color Bar indicates percentage of each pixel showing significant bicoherence at corresponding frequencies. Note the interactions at Alpha Band (8-12 Hz).

ISBN 978-90-827970-1-5 © EURASIP 2018

The confidence level matrix on the other hand, shows interactions gathered around the main diagonal ($f_1 = f_2$). Fig. 6 shows one-sided confidence level matrix averaged across 89 subjects. It is observed that the confidence level tends to increase as the slices approach the main diagonal and maximizes at the main diagonal, reaching double the confidence level of non-diagonal components. Increase in the confidence level suggests an increase in the information content.

Confidence levels located in each slice is averaged in order to investigate the distribution further. The reduced confidence level graph is shown at Fig. 7. It is important to note that the first 4 slices have higher confidence level and the confidence level decreases gradually until the 5th slice. The ratio of decrease is much less after the 4th slice and the confidence level tends to maintain throughout the rest of the matrix. Authors attribute this pattern to 4 Hz. frequency resolution. In order to evaluate the information content of components at the main diagonal, first 4 slices are identified as the diagonal components and the rest of the components are identified as non-diagonal components.

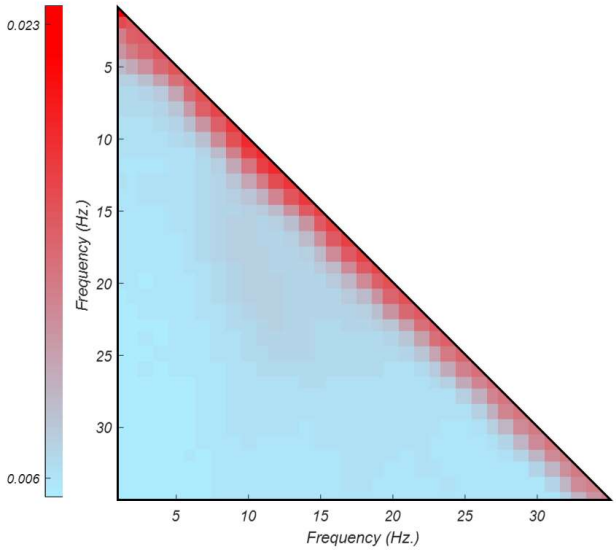

Fig. 6. Empirically Calculated %95 Confidence Level Matrix. Color Bar indicates confidence level averaged across subjects. Confidence level increases as the slices approach the main diagonal, reaching double the confidence level of non-diagonal components.

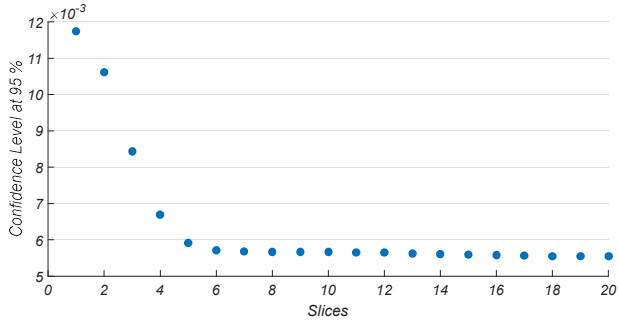

Fig. 7. Reduced Confidence Level. First 4 slices belonging to the main digonal show higher confidence levels. The number of slices is due to 4 Hz spectral resolution limit of bicoherence estimation.

Mean and Standard Error of diagonal and non-diagonal components are given at Fig. 8. We evaluated the information content of bicoherence matrix for each subject and each AVOI. As the figures also suggest, one-tailed t-tests for each condition rejected the null-hypothesis (p<0.05), implying a clear separation in means of information content between diagonal and non-diagonal components.

IV. Conclusion

Results showed that the most prominent nonlinear interactions, particularly QPC is found on the main diagonal and 'sliced bicoherence' is a sufficient method to evaluate 2nd order nonlinear interactions within the resting-state brain. Hence a reduction in the computational burden is possible by using efficient estimation methods suggested by [16]. This does not mean to suggest that the rest of the bicoherence matrix should be ignored especially for other brain conditions. Further studies at different paradigms are required to uncover the true nature of the main diagonal slice of the bicoherence matrix.

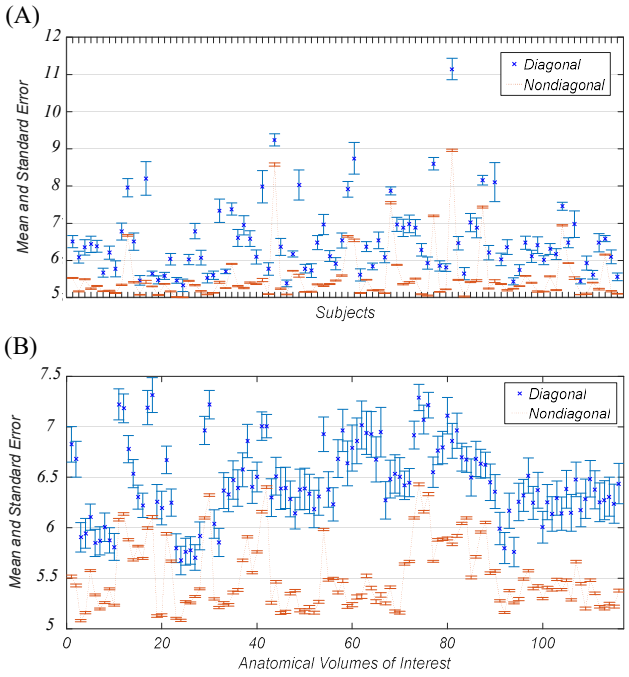

Fig. 8. Mean and Standard Error of Diagonal and Non-Diagonal Components at both subject (A) and AVOI level (B). Mean and Standard Error indicates percentage of cross-coupling at either diagonal frequencies or non-diagonal frequencies. Figures show clear separation between diagonal and non-diagonal components in means of information content.

V. References

[1] K. Friston, "Functional and effective connectivity: a review," *Brain Connectivity,* vol. 1, no. 1, pp. 13-36, 2011.

[2] A. Schnitzler and J. Gross, "Normal and pathological oscillatory communication in the brain," *Nature Reviews Neuroscience,* vol. 6, pp. 285-296, 2005.

[3] P. Fries, "A mechanism for cognitive dynamics: neuronal communication through neuronal coherence," *Trends in Cognitive Science,* vol. 9, no. 10, pp. 474-480, 2005.

ISBN 978-90-827970-1-5 © EURASIP 2018

[4] E. Salinas and T. J. Sejnowski, "Correlated Neuronal Activity and the Flow of Neural Information," *Natura Reviews Neuroscience,* vol. 2, no. 8, pp. 539-550, 2001.

[5] D. M. Halliday, J. R. Rosenberg, A. M. Amjad, P. Breeze, B. A. Conway and S. F. Farmer, "A framework for the analysis of mixed time series/point process data—Theory and application to the study of physiological tremor, single motor unit discharges and electromyograms," *Progress in Biophysics and Molecular Biology,* vol. 64, no. 2-3, pp. 237-278, 1995.

[6] S. M. Bowyer, "Coherence a measure of the brain networks: past and present," *Neuropsychiatric Electrophysiology,* vol. 2016, no. 2:1, pp. 1-12, 2016.

[7] S. Aydore, D. Pantazis and R. M. Leahy, "A note on the phase locking value and its properties," *NeuroImage,* vol. 74, pp. 231-244, 2013.

[8] V. Jirsa and V. Müller, "Cross-frequency coupling in real and virtual brain networks," *Frontiers in Computational Neuroscience,* vol. 7, p. 78, 2013.

[9] T. E. Özkurt and A. Schnitzler, "A critical note on the definition of phase–amplitude cross-frequency coupling," *Journal of Neuroscience Methods,* vol. 201, no. 2, pp. 438-443, 2011.

[10] E. Florin and S. Baillet, "The brain's resting-state activity is shaped by synchronized cross-frequency coupling of neural oscillations," *NeuroImage,* vol. 111, pp. 26-35, 2015.

[11] G. L. Colclough, M. W. Woolrich, P. Tewarie, M. J. Brookes, A. J. Quinn and S. M. Smith, "How reliable are MEG resting-state connectivity metrics?," *NeuroImage,* vol. 138, pp. 284-293, 2016.

[12] P. Venkatakrishnan, R. Sukanesh and S. Sangeetha, "Detection of quadratic phase coupling from human EEG signals using higher order statistics and spectra," *Signal Image and Video Processing,* vol. 5, no. 2, pp. 217-229, 2011.

[13] T. P. Barnett, L. C. Johnson, P. Naitoh, N. Hicks and C. Nute, "Bispectrum Analysis of Electroencephalogram Signals during Waking and Sleeping," *Science,* vol. 172, no. 3981, pp. 401-402, 1971.

[14] G. Dumermuth, P. J. Huber, B. Kleiner and T. Gasser, "Analysis of the interrelations between frequency bands of the EEG by means of the bispectrum a preliminary study," *Electroencephalography and Clinical Neurophysiology,* vol. 31, no. 2, pp. 137-148, 1971.

[15] C. L. Nikias and J. M. Mendel, "Signal processing with higher-order spectra," *IEEE Signal Processing Magazine,* vol. 10, no. 3, pp. 10-37, 1993.

[16] T. E. Özkurt, "Estimation of nonlinear neural source interactions via sliced bicoherence," *Biomedical Signal Processing and Control,* vol. 30, pp. 43-52, 2016.

[17] F. Chella, L. Marzetti, V. Pizzella, F. Zappasodi and G. Nolte, "Third order spectral analysis robust to mixing artifacts for mapping cross-frequency interactions in EEG/MEG," *NeuroImage,* vol. 91, pp. 146-161, 2014.

[18] X. Wang, Y. Chen and M. Ding, "Testing for Statistical Significance in Bispectra: A Surrogate Data Approach and Application to Neuroscience", *IEEE Transactions on Biomedical Engineering*, vol. 54, no. 11, 2007.

[19] F. Shahbazi, A. Ewald and G. Nolte, "Univariate normalization of bispectrum using Hölder's inequality," *Journal of Neuroscience Methods,* vol. 233, pp. 177-186, 2014.

[20] E. Wodey, O. Tirel, J. Y. Bansard, A. Terrier, C. Chanavaz, R. Harris, C. Ecoffey, L. Senhadji, “Impact of age on both BIS values and EEG bispectrum during anaesthesia with sevoflurane in children,” *British Journal of Anaesthesia*, vol. 94, pp. 810-820, 2005.

[21] D. Van Essen, S. Smith, D. Barch, T. Behrens, E. Yacoub, K. Ugurbil and WU-Minn HCP Consortium, "The WU-Minn Human Connectome Project: an overview.," *Neuroimage,* vol. 80, pp. 62-79, 2013.

[22] WU-Minn HCP Consortium, "Human Connectome Project 1200 Subjects Data Release Reference Manual," 2017.

[23] R. Oostenveld, P. Fries, E. Maris and J.-M. Schoffelen, "FieldTrip: Open Source Software for Advanced Analysis of MEG, EEG, and Invasive Electrophysiological Data," *Computational Intelligence and Neuroscience,* vol. 2011, 2011.

[24] A. Swami, J. M. Mendel and C. L. Nikias, "Higher-Order Spectral Analysis Toolbox," United Signals & Systems, Inc., 1993.

[25] N. Tzourio-Mazoyer, B. Landeau, D. Papathanassiou, F. Crivello, O. Etard, N. Delcroix, B. Mazoyer and M. Joliot, "Automated anatomical labeling of activations in SPM using a macroscopic anatomical parcellation of the MNI MRI single-subject brain.," *Neuroimage,* vol. 15, no. 1, pp. 273-289, 2002.

[26] B. Van Veen, W. van Drongelen, M. Yuchtman and A. Suzuki, "Localization of brain electrical activity via linearly constrained minimum variance spatial filtering," *IEEE Transactions on Biomedical Engineering,* vol. 44, no. 9, pp. 867-880, 1997.

[27] S. Elgar, C. W. Van Atta and M. Gharib, "Cross-bispectral analysis of a vibrating cylinder and its wake in low Reynolds number flow," *Journal of Fluids and Structures,* vol. 4, no. 1, pp. 59-71, 1990.

[28] B. Efron, "Bootstrap Methods: Another Look at the Jackknife," Stanford University, 1979.

ISBN 978-90-827970-1-5 © EURASIP 2018